IEEE Access
Multidisciplinary | Rapid Review | Open Access Journal

Received November 19, 2020, accepted November 24, 2020, date of publication November 27, 2020,
date of current version December 31, 2020.

Digital Object Identifier 10.1109/ACCESS.2020.3041009

Stochastic Cramer-Rao Bound for DOA Estimation With a Mixture of Circular and Noncircular Signals

JINGJING CAI[1], YIBAO LIANG[2], WEI LIU[3], (Senior Member, IEEE), AND YANG-YANG DONG[1], (Member, IEEE)

[1]School of Electronic Engineering, Xidian University, Xi'an 710071, China
[2]School of Information and Electronics, Beijing Institute of Technology, Beijing 100081, China
[3]Department of Electronic and Electrical Engineering, The University of Sheffield, Sheffield S1 3JD, U.K.

Corresponding author: Jingjing Cai (jjcai@mail.xidian.edu.cn)

This work was supported in part by the National Natural Science Foundation of China under Grant 61805189 and Grant 61901332, in part by the Natural Science Basic Research Plan in Shaanxi Provincial of China under Grant 2018JQ6068, and in part by the Fundamental Research Funds for the Central Universities under Grant JB190201.

ABSTRACT The Cramer-Rao bound (CRB) offers insights into the inherent performance benchmark of any unbiased estimator developed for a specific parametric model, which is an important tool to evaluate the performance of direction-of-arrival (DOA) estimation algorithms. In this paper, a closed-form stochastic CRB for a mixture of circular and noncircular uncorrelated Gaussian signals is derived. As a general one, it can be transformed into some existing representative results. The existence condition of the CRB is also analysed based on sparse arrays, which allows the number of signals to be more than the number of physical sensors. Finally, numerical comparisons are conducted in various scenarios to demonstrate the validity of the derived CRB.

INDEX TERMS Cramer-Rao bound, direction of arrival, circular and noncircular, sparse arrays.

I. INTRODUCTION

Direction of arrival (DOA) estimation based on sensor arrays has been of great interest in many applications, such as radar, sonar, and wireless communications. A common tool to assess the performance of DOA estimation algorithms is the Cramer-Rao bound (CRB), which provides a lower bound on the estimation error (mean squared error) of an unbiased DOA estimator. According to the probability model of the source signals, the CRB can be classified into the deterministic CRB [1] and the stochastic one [2].

Although the CRB for all unknown parameters can be obtained from the inverse of the Fisher information matrix (FIM), this process tends to involve complicated matrix manipulations. In many cases, we are only interested in the CRB for DOA estimation, and a closed-form CRB for DOA estimation not only avoids calculation of the nuisance parameters, but also provides analytical insights into the dependence of the array performance on different parameters [1]–[20].

The associate editor coordinating the review of this manuscript and approving it for publication was Mohammad Zia Ur Rahman.

In the past years, various sparse array structures have been investigated extensively, as they can provide much more degrees of freedom (DOFs) than traditional uniform linear arrays (ULAs). Two representative sparse array structures are the co-prime arrays [21]–[23] and nested arrays [24], [25]. Many methods have been proposed for DOA estimation based on such arrays, which can estimate more sources than the number of physical sensors by exploiting the difference coarrays [21], [22], [26]–[32]. At the same time, the CRB especially applied to sparse arrays has also been derived [3]–[6], and the existence conditions of these CRBs imply that more sources than the number of physical sensors can be identified by using sparse arrays.

However, most of the studies based on sparse arrays do not consider the possible noncircularity of the impinging signals. In practice, noncircular signals are frequently used, and some representative examples include signals generated by the following modulation schemes: binary phase shift keying (BPSK), amplitude shift keying (ASK), pulse amplitude modulation (PAM) and unbalanced quadrature phase shift keying (UQPSK). The second-order statistical properties of circular signals are characterized by the covariance matrix,

while those of noncircular signals are determined by both the covariance and pseudo covariance matrices.

For traditional arrays, many efforts have been made to explicitly exploit the noncircularity of the signals to improve the performance of parameter estimation [31], [33]–[43], some of which also examined the CRB for noncircular signals in various scenarios. For Gaussian noncircular signals, the stochastic CRB has been derived in different noise fields [7]–[9]. In particular, for discrete BPSK and quadrature phase shift keying (QPSK) signals, the stochastic CRB was derived in [10]. For strictly noncircular (rectilinear) signals, the stochastic CRB was derived in [11], while the deterministic one was investigated in [40]. Moreover, for a mixture of circular and noncircular signals, only the deterministic CRB has been studied in [12], [13], whereas the stochastic one is unavailable in the literature.

Most recently, several algorithms were proposed to deal with the DOA estimation problem for a mixture of circular and noncircular signals [31], [44]. Benefiting from the enhanced DOFs of sparse arrays, these algorithms make use of the *a priori* knowledge of uncorrelated sources, and are able to identify much more sources than the number of physical sensors. When assessing the performance of these algorithms, existing results on the stochastic noncircular CRBs are not applicable, because they are either restricted by the condition that the number of sources is strictly less than that of physical sensors [7], [8], or derived for strictly noncircular signals only [11]. Moreover, in the derivation of these results, all the unknown entries in the source covariance matrix are considered as part of the unknown parameters. However, under such parameterization, the role of those parameters associated with noncircularity are not highlighted.

As the deterministic model is independent of the noncircularity of signals [7], [9], and the corresponding CRB does not exist in the underdetermined case [3], we shall focus on the stochastic model, based on which all the underdetermined DOA estimation methods are developed. In this work, a closed-form stochastic CRB for a mixture of circular and noncircular signals is derived for the first time, and in particular its application to sparse arrays is discussed. The main contributions of our work are stated in the following.

1) The derived stochastic CRB is applicable to various array geometries, such as ULAs, sparse arrays, and circular arrays, as long as there is only one unknown parameter associated with each source. Since a mixture of circular and noncircular signals is assumed, the derived CRB can be easily modified to fit some existing ones derived for circular/noncircular signals only as special cases. Moreover, our CRB expression is applicable to cases with more sources than the number of physical sensors, whereas the traditional noncircular CRBs in [7], [8] turn out to be invalid.
2) Based on a general signal model for arbitrary second-order noncircularity, a different parameterization is used to derive the CRB. Compared with the traditional parameterization in [7], [8], ours highlights the roles of the noncircularity phase and the noncircularity rate, which further improves the DOA estimation accuracy.
3) Considering practical applications of sparse arrays, the existence condition of the derived CRB is examined, and the maximum number of resolvable sources is deduced. We show that much more noncircular Gaussian sources than sensors can be resolved due to the enhanced DOFs provided by sparse arrays. For a given sparse array, the upper bound on the number of resolvable circular sources can be exceeded when noncircularity is considered.

The rest of this paper is organized as follows. The general data model and the sensor array signal model are introduced in Sec. II. The closed-form stochastic CRB expression is derived in Sec. III. The existence condition of the CRB is presented in Sec. IV. Numerical results are provided in Sec. V and conclusions are drawn in Sec. VI.

II. DATA MODEL

A. GENERAL SOURCE MODEL WITH ARBITRARY SECOND-ORDER NONCIRCULARITY

First, a quick review of a general signal model for arbitrary second-order noncircularity is provided.

Denote $s_i(k)$ as the ith ($i = 1, 2, \ldots, N$) narrowband source signal corresponding to the kth ($k = 1, 2, \ldots, K$) time instant. In linear digital modulation schemes, the in-phase component $s_{I_i}(k)$ and the quadrature component $s_{Q_i}(k)$ of the complex-valued signal $s_i(k)$ are often uncorrelated, leading to $E\{s_{I_i}(k)s_{Q_i}(k)\} = 0$ [45].

Consider a normalised version of the signal, i.e.

$$E\{s_i(k)s_i^*(k)\} = 1, \tag{1}$$

and in general, we have

$$E\{s_i^2(k)\} = \rho_i e^{j\psi_i}, \tag{2}$$

where $E\{\cdot\}$ is the expectation operation, ψ_i is referred to as the noncircularity phase, and ρ_i the noncircularity rate.

According to different choices of the noncircularity rate ρ_i, we have the following three types of signals.

1) Circular signals: $\rho_i = 0$. As a result, the pseudo covariance becomes $E\{s_i^2(k)\} = 0$. One example for this case is the QPSK signal.
2) Strictly noncircular signals: $\rho_i = 1$. The pseudo covariance becomes $E\{s_i^2(k)\} = e^{j\psi_i}$. Three examples are BPSK, PAM and ASK signals.
3) Nonstrictly noncircular signals: $0 < \rho_i < 1$. The pseudo covariance becomes $E\{s_i^2(k)\} = \rho_i e^{j\psi_i}$. One example for this case is the UQPSK signal.

B. SENSOR ARRAY SIGNAL MODEL

Consider an array consisting of M sensors receiving N stationary narrowband source signals in the far-field. The sources are located at distinct directions $\boldsymbol{\theta} = [\theta_1, \theta_2, \ldots, \theta_N]^T$ with $(\cdot)^T$ denoting the transpose operation. The source powers are denoted by $\boldsymbol{\mu} = [\mu_1, \mu_2, \ldots, \mu_N]^T$.

The kth snapshot of the output signal at the mth sensor corresponding to the ith source can be expressed as [27], [28], [31]

$$y_m(k) = \sum_{i=1}^{N} a_m(\theta_i)s_i(k) + n_m(k), \quad m = 1, 2, \ldots, M. \quad (3)$$

where $a_m(\theta_i)$ is the response of the mth sensor to the ith source, $n_m(k)$ denotes the noise at the mth sensor, which is uncorrelated with the sources signals.

The received array signal vector is given by

$$\mathbf{y}(k) = \sum_{i=1}^{N} \mathbf{a}(\theta_i)s_i(k) + \mathbf{n}(k) = \mathbf{A}(\boldsymbol{\theta})\mathbf{s}(k) + \mathbf{n}(k), \quad (4)$$

with

$$\begin{aligned} \mathbf{s}(k) &= [s_1(k), s_2(k), \ldots, s_N(k)]^T, \\ \mathbf{n}(k) &= [n_1(k), n_2(k), \ldots, n_M(k)]^T, \\ \mathbf{A}(\boldsymbol{\theta}) &= [\mathbf{a}(\theta_1), \mathbf{a}(\theta_2), \ldots, \mathbf{a}(\theta_N)], \\ \mathbf{a}(\theta_i) &= [a_1(\theta_i), a_2(\theta_i), \ldots, a_M(\theta_i)]^T, \end{aligned} \quad (5)$$

where $\mathbf{s}(k)$ is the source signal vector, and $\mathbf{n}(k)$ is the noise vector. $\mathbf{A}(\boldsymbol{\theta})$ and $\mathbf{a}(\theta_i)$ represent the array steering matrix and the steering vector of the ith source, respectively.

The source signals are assumed to be a mixture of circular and noncircular ones, mutually uncorrelated. The first N_{nc} ones are noncircular Gaussian distributed with zero mean, while the remaining N_{nc} ones are circular Gaussian distributed with zero mean (such information can be available and has been used by some algorithms, e.g., [46]). The noise is assumed to be spatially uncorrelated, circular Gaussian distributed with zero mean, with its power denoted by σ^2.

From (1), the covariance matrix and pseudo covariance matrix of the received array signals are respectively given by

$$\begin{aligned} \mathbf{R}_{\text{d}} &= E\{\mathbf{y}(k)\mathbf{y}^H(k)\} \\ &= \sum_{i=1}^{N} E\{s_i(k)s_i^*(k)\}\mathbf{a}(\theta_i)\mathbf{a}^H(\theta_i) + \sigma^2\mathbf{I}_M \\ &= \sum_{i=1}^{N} \mu_i\mathbf{a}(\theta_i)\mathbf{a}^H(\theta_i) + \sigma^2\mathbf{I}_M, \\ \mathbf{R}_{\text{s}} &= E\{\mathbf{y}(k)\mathbf{y}^T(k)\} = \sum_{i=1}^{N} E\{s_i^2(k)\}\mathbf{a}(\theta_i)\mathbf{a}^T(\theta_i) \\ &= \sum_{i=1}^{N_{\text{nc}}} \mu_i\rho_i e^{\text{j}\psi_i}\mathbf{a}(\theta_i)\mathbf{a}^T(\theta_i). \end{aligned} \quad (6)$$

where $(\cdot)^H$ denotes the Hermitian transpose operation and $\mathbf{I}_M$ is an $M \times M$ identity matrix.

III. STOCHASTIC CRB FOR A MIXTURE OF CIRCULAR AND NONCIRCULAR GAUSSIAN SIGNALS

A. DERIVATION OF THE STOCHASTIC CRB

By definition, the CRB is obtained from the inverse of the Fisher information matrix (FIM). For Gaussian distributed data, the FIM can be conveniently calculated from the Slepian-Bangs formula [47], [48]. The most popular version is derived for circular Gaussian signals, according to which the (p, q)th entry of the FIM is expressed as [2], [4], [5]

$$\left[\mathbf{F}_{\text{d}}(\boldsymbol{\xi}_{\text{d}})\right]_{p,q} = Ktr\left(\mathbf{R}_{\text{d}}^{-1}\frac{\partial\mathbf{R}_{\text{d}}}{\partial[\boldsymbol{\xi}_{\text{d}}]_p}\mathbf{R}_{\text{d}}^{-1}\frac{\partial\mathbf{R}_{\text{d}}}{\partial[\boldsymbol{\xi}_{\text{d}}]_q}\right). \quad (7)$$

where

$$\boldsymbol{\xi}_{\text{d}} = [\boldsymbol{\theta}^T, \boldsymbol{\mu}^T, \sigma^2]^T. \quad (8)$$

Here, $\boldsymbol{\xi}_{\text{d}}$ is the vector holding all real-valued unknown parameters, and $tr(\cdot)$ stands for the trace operation.

Taking into account noncircular signals, the conjugate of the received array signals also contains useful information. Let $\mathbf{R}_{\text{e}}$ denote the covariance matrix of the augmented array signal vector $\mathbf{y}_{\text{e}}(k) = [\mathbf{y}^T(k), \mathbf{y}^H(k)]^T$, and then $\mathbf{R}_{\text{e}}$ can be constructed by $\mathbf{R}_{\text{d}}$ and $\mathbf{R}_{\text{s}}$ in (6) as follows

$$\mathbf{R}_{\text{e}} = \begin{bmatrix} \mathbf{R}_d & \mathbf{R}_s \\ \mathbf{R}_s^* & \mathbf{R}_d^* \end{bmatrix}. \quad (9)$$

Let $\boldsymbol{\xi}_{\text{e}}$ denote the extended unknown parameter vector which includes not only the DOAs, the source powers and the noise power, but also the noncircularity phase and the noncircularity rate:

$$\begin{aligned} \boldsymbol{\xi}_{\text{e}} &= [\boldsymbol{\theta}^T, \boldsymbol{\mu}^T, \boldsymbol{\psi}^T, \boldsymbol{\rho}^T, \sigma^2]^T, \\ \boldsymbol{\theta} &= [\boldsymbol{\theta}_{\text{nc}}^T, \boldsymbol{\theta}_{\text{c}}^T]^T, \quad \boldsymbol{\mu} = [\boldsymbol{\mu}_{\text{nc}}^T, \boldsymbol{\mu}_{\text{c}}^T]^T, \\ \boldsymbol{\theta}_{\text{nc}} &= [\theta_1, \theta_2 \ldots, \theta_{N_{\text{nc}}}]^T, \\ \boldsymbol{\theta}_{\text{c}} &= [\theta_{N_{\text{nc}}+1}, \theta_{N_{\text{nc}}+2} \ldots, \theta_N]^T, \\ \boldsymbol{\mu}_{\text{nc}} &= [\mu_1, \mu_2 \ldots, \mu_{N_{\text{nc}}}]^T, \\ \boldsymbol{\mu}_{\text{c}} &= [\mu_{N_{\text{nc}}+1}, \mu_{N_{\text{nc}}+2} \ldots, \mu_N]^T, \\ \boldsymbol{\psi} &= [\psi_1, \psi_2, \ldots, \psi_{N_{\text{nc}}}]^T, \\ \boldsymbol{\rho} &= [\rho_1, \rho_2, \ldots, \rho_{N_{\text{nc}}}]^T. \end{aligned} \quad (10)$$

Remark 1: If we adopt the parameterization in [7], [8], the unknown parameter vector should be written as

$$\boldsymbol{\xi}_{\text{Del}} = \left[\boldsymbol{\theta}^T, \boldsymbol{\mu}^T, \text{Re}(\mathbf{p}_{\text{s}}^T), \text{Im}(\mathbf{p}_{\text{s}}^T), \sigma^2\right]^T, \quad (11)$$

where $\mathbf{p}_{\text{s}}$ is a column vector collecting the diagonal entries of the pseudo covariance matrix of the noncircular source signals, and $\text{Re}(\cdot)$ and $\text{Im}(\cdot)$ are the real and imaginary parts of the input argument, respectively. Note that the total number of unknowns in $\boldsymbol{\xi}_{\text{e}}$ and $\boldsymbol{\xi}_{\text{Del}}$ are both $2N+2N_{\text{nc}}+1$. Compared to $\boldsymbol{\xi}_{\text{Del}}$, the advantage of $\boldsymbol{\xi}_{\text{e}}$ is that the roles of the noncircularity phase and the noncircularity rate ($\boldsymbol{\psi}$ and $\boldsymbol{\rho}$) can be highlighted in the derivation and analysis of CRB, as will be shown next.

Since the boundary of the probability density function (p.d.f.) of $\mathbf{y}_{\text{e}}(k)$ is independent of $\boldsymbol{\xi}_{\text{e}}$, the following regularity condition holds true

$$E\left\{\frac{\partial \ln f[\mathbf{y}_{\text{e}}(k); \boldsymbol{\xi}_{\text{e}}]}{\partial \boldsymbol{\xi}_{\text{e}}^T}\right\} = \mathbf{0}, \quad (12)$$

where $\ln f[\mathbf{y}_{\text{e}}(k); \boldsymbol{\xi}_{\text{e}}]$ is the log-p.d.f. of $\mathbf{y}_{\text{e}}(k)$, and $\partial f/\partial\boldsymbol{\xi}_{\text{e}}^T$ represents the derivatives of a function f with respect

to $\boldsymbol{\xi}_{\mathrm{e}}^T$. According to the extended Slepian-Bangs formula for the noncircular complex Gaussian distribution with zero mean [8], we can write the (p, q)th entry of the FIM as

$$\begin{aligned}\left[\mathbf{F}_{\mathrm{e}}(\boldsymbol{\xi}_{\mathrm{e}})\right]_{p,q} &= \frac{K}{2}\mathrm{tr}\left(\mathbf{R}_e^{-1}\frac{\partial \mathbf{R}_e}{\partial [\boldsymbol{\xi}_{\mathrm{e}}]_p}\mathbf{R}_e^{-1}\frac{\partial \mathbf{R}_e}{\partial [\boldsymbol{\xi}_{\mathrm{e}}]_q}\right)\\ &= \frac{K}{2}\left[(\mathbf{R}_{\mathrm{e}}^T\otimes\mathbf{R}_{\mathrm{e}})^{-\frac{1}{2}}\frac{\partial \mathbf{r}_{\mathrm{e}}}{\partial [\boldsymbol{\xi}_{\mathrm{e}}]_p}\right]^H\left[(\mathbf{R}_{\mathrm{e}}^T\otimes\mathbf{R}_{\mathrm{e}})^{-\frac{1}{2}}\frac{\partial \mathbf{r}_{\mathrm{e}}}{\partial [\boldsymbol{\xi}_{\mathrm{e}}]_q}\right],\end{aligned} \tag{13}$$

where $\otimes$ denotes the Kronecker product, and

$$\mathbf{r}_{\mathrm{e}} = \mathrm{vec}(\mathbf{R}_{\mathrm{e}}), \tag{14}$$

with $\mathrm{vec}(\cdot)$ denoting the vectorization operation.

Introduce the following notations

$$\begin{aligned}\mathbf{W}_{\mathrm{e}} &= (\mathbf{R}_{\mathrm{e}}^T\otimes\mathbf{R}_{\mathrm{e}})^{-\frac{1}{2}},\quad \mathbf{G}_{\mathrm{e}} = \mathbf{W}_{\mathrm{e}}\frac{\partial \mathbf{r}_{\mathrm{e}}}{\partial \boldsymbol{\theta}^T},\\ \mathbf{Q}_{\mathrm{e}} &= \mathbf{W}_{\mathrm{e}}\left[\frac{\partial \mathbf{r}_{\mathrm{e}}}{\partial \boldsymbol{\mu}^T},\quad \frac{\partial \mathbf{r}_{\mathrm{e}}}{\partial \boldsymbol{\psi}^T},\ \frac{\partial \mathbf{r}_{\mathrm{e}}}{\partial \boldsymbol{\rho}^T},\ \frac{\partial \mathbf{r}_{\mathrm{e}}}{\partial \sigma^2}\right].\end{aligned} \tag{15}$$

The dimensions of $\mathbf{G}_{\mathrm{e}}$ and $\mathbf{Q}_{\mathrm{e}}$ are $4M^2\times N$ and $4M^2\times(N+2N_{\mathrm{nc}}+1)$, receptively. Therefore, we can rewrite $\mathbf{F}_{\mathrm{e}}(\boldsymbol{\xi}_{\mathrm{e}})$ as

$$\mathbf{F}_{\mathrm{e}}(\boldsymbol{\xi}_{\mathrm{e}}) = \frac{K}{2}\begin{bmatrix}\mathbf{G}_{\mathrm{e}}^H\mathbf{G}_{\mathrm{e}} & \mathbf{G}_{\mathrm{e}}^H\mathbf{Q}_{\mathrm{e}}\\ \mathbf{Q}_{\mathrm{e}}^H\mathbf{G}_{\mathrm{e}} & \mathbf{Q}_{\mathrm{e}}^H\mathbf{Q}_{\mathrm{e}}\end{bmatrix}. \tag{16}$$

To facilitate the calculation of $\mathbf{G}_{\mathrm{e}}$ and $\mathbf{Q}_{\mathrm{e}}$, we write $\mathbf{r}_{\mathrm{e}}$ as

$$\mathbf{r}_{\mathrm{e}} = \mathbf{P}[\mathbf{r}_{\mathrm{d}}^T, \mathbf{r}_{\mathrm{s}}^H, \mathbf{r}_{\mathrm{s}}^T, \mathbf{r}_{\mathrm{d}}^H]^T, \tag{17}$$

where

$$\begin{aligned}\mathbf{P} &= \left[\mathbf{I}_2\otimes\left(\sum_{m=1}^{M}\sum_{j=1}^{2}\mathbf{B}_{m,j}\otimes\mathbf{B}_{m,j}^T\right)\otimes\mathbf{I}_M\right]^{-1},\\ \mathbf{r}_{\mathrm{d}} &= \mathrm{vec}(\mathbf{R}_{\mathrm{d}}) = \mathbf{T}_{\mathrm{d}}(\boldsymbol{\theta})\boldsymbol{\mu}+\sigma^2\mathrm{vec}(\mathbf{I}_M),\\ \mathbf{r}_{\mathrm{s}} &= \mathrm{vec}(\mathbf{R}_{\mathrm{s}}) = \mathbf{T}_{\mathrm{s}}(\boldsymbol{\theta}_{\mathrm{nc}})\mathrm{diag}(\boldsymbol{\mu}_{\mathrm{nc}})\mathrm{diag}(\boldsymbol{\rho})\boldsymbol{\psi}_{\mathrm{e}},\\ \mathbf{T}_{\mathrm{d}}(\boldsymbol{\theta}) &= \mathbf{A}^*(\boldsymbol{\theta})\odot\mathbf{A}(\boldsymbol{\theta}),\\ \mathbf{T}_{\mathrm{s}}(\boldsymbol{\theta}_{\mathrm{nc}}) &= \mathbf{A}(\boldsymbol{\theta}_{\mathrm{nc}})\odot\mathbf{A}(\boldsymbol{\theta}_{\mathrm{nc}}),\\ \boldsymbol{\psi}_{\mathrm{e}} &= \left[\mathrm{e}^{\mathrm{j}\psi_1}, \mathrm{e}^{\mathrm{j}\psi_2}, \ldots, \mathrm{e}^{\mathrm{j}\psi_{N_{\mathrm{nc}}}}\right].\end{aligned} \tag{18}$$

Here, $\mathbf{B}_{m,j}$ is an $M\times 2$ matrix with one at the (m,j)th position and zeros elsewhere, $\odot$ denotes the Khatri-Rao product (column-wise Kronecker product), and $\mathrm{diag}(\cdot)$ refers to a diagonal matrix whose diagonal entries are given by the input vector.

Substituting (17) into (15), we can rewrite $\mathbf{G}_{\mathrm{e}}$ and $\mathbf{Q}_{\mathrm{e}}$ as

$$\mathbf{G}_{\mathrm{e}} = \mathbf{W}_{\mathrm{e}}\mathbf{P}\left[\left(\frac{\partial \mathbf{r}_{\mathrm{d}}}{\partial \boldsymbol{\theta}^T}\right)^T, \left(\frac{\partial \mathbf{r}_{\mathrm{s}}^*}{\partial \boldsymbol{\theta}^T}\right)^T, \left(\frac{\partial \mathbf{r}_{\mathrm{s}}}{\partial \boldsymbol{\theta}^T}\right)^T, \left(\frac{\partial \mathbf{r}_{\mathrm{d}}^*}{\partial \boldsymbol{\theta}^T}\right)^T\right]^T,$$

$$\mathbf{Q}_{\mathrm{e}} = \mathbf{W}_{\mathrm{e}}\mathbf{P}\begin{bmatrix}\frac{\partial \mathbf{r}_{\mathrm{d}}}{\partial \boldsymbol{\mu}^T} & \frac{\partial \mathbf{r}_{\mathrm{d}}}{\partial \boldsymbol{\psi}^T} & \frac{\partial \mathbf{r}_{\mathrm{d}}}{\partial \boldsymbol{\rho}^T} & \frac{\partial \mathbf{r}_{\mathrm{d}}}{\partial \sigma^2}\\ \frac{\partial \mathbf{r}_{\mathrm{s}}^*}{\partial \boldsymbol{\mu}^T} & \frac{\partial \mathbf{r}_{\mathrm{s}}^*}{\partial \boldsymbol{\psi}^T} & \frac{\partial \mathbf{r}_{\mathrm{s}}^*}{\partial \boldsymbol{\rho}^T} & \frac{\partial \mathbf{r}_{\mathrm{s}}^*}{\partial \sigma^2}\\ \frac{\partial \mathbf{r}_{\mathrm{s}}}{\partial \boldsymbol{\mu}^T} & \frac{\partial \mathbf{r}_{\mathrm{s}}}{\partial \boldsymbol{\psi}^T} & \frac{\partial \mathbf{r}_{\mathrm{s}}}{\partial \boldsymbol{\rho}^T} & \frac{\partial \mathbf{r}_{\mathrm{s}}}{\partial \sigma^2}\\ \frac{\partial \mathbf{r}_{\mathrm{d}}^*}{\partial \boldsymbol{\mu}^T} & \frac{\partial \mathbf{r}_{\mathrm{d}}^*}{\partial \boldsymbol{\psi}^T} & \frac{\partial \mathbf{r}_{\mathrm{d}}^*}{\partial \boldsymbol{\rho}^T} & \frac{\partial \mathbf{r}_{\mathrm{d}}^*}{\partial \sigma^2}\end{bmatrix}. \tag{19}$$

Using (18), we can compute the derivatives in (19), and the results are listed below.

$$\begin{aligned}\frac{\partial \mathbf{r}_{\mathrm{d}}}{\partial \boldsymbol{\theta}^T} &= [\mathbf{T}_{\mathrm{d}}'(\boldsymbol{\theta}_{\mathrm{nc}})\mathrm{diag}(\boldsymbol{\mu}_{\mathrm{nc}}), \mathbf{T}_{\mathrm{d}}'(\boldsymbol{\theta}_{\mathrm{c}})\mathrm{diag}(\boldsymbol{\mu}_{\mathrm{c}})],\\ \frac{\partial \mathbf{r}_{\mathrm{d}}}{\partial \boldsymbol{\mu}^T} &= [\mathbf{T}_{\mathrm{d}}(\boldsymbol{\theta}_{\mathrm{nc}}), \mathbf{T}_{\mathrm{d}}(\boldsymbol{\theta}_{\mathrm{c}})],\quad \frac{\partial \mathbf{r}_{\mathrm{d}}}{\partial \boldsymbol{\psi}^T} = \mathbf{0}_{M^2\times N_{\mathrm{nc}}},\\ \frac{\partial \mathbf{r}_{\mathrm{d}}}{\partial \boldsymbol{\rho}^T} &= \mathbf{0}_{M^2\times N_{\mathrm{nc}}},\quad \frac{\partial \mathbf{r}_{\mathrm{d}}}{\partial \sigma^2} = \mathrm{vec}(\mathbf{I}_M),\\ \frac{\partial \mathbf{r}_{\mathrm{s}}}{\partial \boldsymbol{\theta}^T} &= \left[\mathbf{T}_{\mathrm{s}}'(\boldsymbol{\theta}_{\mathrm{nc}})\mathrm{diag}(\boldsymbol{\mu}_{\mathrm{nc}})\mathrm{diag}(\boldsymbol{\rho})\mathrm{diag}(\boldsymbol{\psi}_{\mathrm{e}}), \mathbf{0}_{M^2\times N_{\mathrm{c}}}\right],\\ \frac{\partial \mathbf{r}_{\mathrm{s}}}{\partial \boldsymbol{\mu}^T} &= \left[\mathbf{T}_{\mathrm{s}}(\boldsymbol{\theta}_{\mathrm{nc}})\mathrm{diag}(\boldsymbol{\rho})\mathrm{diag}(\boldsymbol{\psi}_{\mathrm{e}}), \mathbf{0}_{M^2\times N_{\mathrm{c}}}\right],\\ \frac{\partial \mathbf{r}_{\mathrm{s}}}{\partial \boldsymbol{\psi}^T} &= \mathrm{j}\mathbf{T}_{\mathrm{s}}(\boldsymbol{\theta}_{\mathrm{nc}})\mathrm{diag}(\boldsymbol{\mu})\mathrm{diag}(\boldsymbol{\rho})\mathrm{diag}(\boldsymbol{\psi}_{\mathrm{e}}),\\ \frac{\partial \mathbf{r}_{\mathrm{s}}}{\partial \boldsymbol{\rho}^T} &= \mathbf{T}_{\mathrm{s}}(\boldsymbol{\theta}_{\mathrm{nc}})\mathrm{diag}(\boldsymbol{\mu})\mathrm{diag}(\boldsymbol{\psi}_{\mathrm{e}}),\quad \frac{\partial \mathbf{r}_{\mathrm{s}}}{\partial \sigma^2} = \mathbf{0}_{M^2\times 1},\end{aligned} \tag{20}$$

where

$$\begin{aligned}\mathbf{T}_{\mathrm{d}}'(\boldsymbol{\theta}) &= \mathbf{A}'^*(\boldsymbol{\theta})\odot\mathbf{A}(\boldsymbol{\theta})+\mathbf{A}^*(\boldsymbol{\theta})\odot\mathbf{A}'(\boldsymbol{\theta}),\\ \mathbf{T}_{\mathrm{s}}'(\boldsymbol{\theta}_{\mathrm{nc}}) &= \mathbf{A}'(\boldsymbol{\theta}_{\mathrm{nc}})\odot\mathbf{A}(\boldsymbol{\theta}_{\mathrm{nc}})+\mathbf{A}(\boldsymbol{\theta}_{\mathrm{nc}})\odot\mathbf{A}'(\boldsymbol{\theta}_{\mathrm{nc}}),\\ \mathbf{A}'(\boldsymbol{\theta}) &= \left[\frac{\partial \mathbf{a}(\theta_1)}{\partial\theta_1}, \frac{\partial \mathbf{a}(\theta_2)}{\partial\theta_2}\ldots, \frac{\partial \mathbf{a}(\theta_N)}{\partial\theta_N}\right].\end{aligned} \tag{21}$$

Assume that $\mathbf{F}_{\mathrm{e}}(\boldsymbol{\xi}_{\mathrm{e}})$ is positive definite. Since we are only interested in the CRB for DOA estimation, the DOA-related block of the CRB matrix can be expressed as

$$\mathrm{CRB}_{\mathrm{e}}(\boldsymbol{\theta}) = \frac{2}{K}(\mathbf{G}_{\mathrm{e}}^H\boldsymbol{\Pi}_{\mathbf{Q}_{\mathrm{e}}}^{\perp}\mathbf{G}_{\mathrm{e}})^{-1}, \tag{22}$$

with

$$\boldsymbol{\Pi}_{\mathbf{Q}_{\mathrm{e}}}^{\perp} = \mathbf{I}_{4M^2}-\mathbf{Q}_{\mathrm{e}}(\mathbf{Q}_{\mathrm{e}}^H\mathbf{Q}_{\mathrm{e}})^{-1}\mathbf{Q}_{\mathrm{e}}^H. \tag{23}$$

B. DISCUSSION ON SPECIAL CASES

The stochastic CRB expression in (22) is a general one suitable for various array geometries, as long as there is only one parameter to be estimated for each source. Moreover, it can be easily modified to fit the following special cases.

1) All the source signals are known to be circular. In this case, $\mathbf{R}_{\mathrm{s}} = \mathbf{0}$, and then (13) degenerates to (7). From this point of view, the circular CRB can be seen as a special case of the noncircular CRB. Specifically, the newly constructed $\mathbf{G}_d$ and $\mathbf{Q}_d$ can be written as

$$\begin{aligned}\mathbf{G}_d &= (\mathbf{R}_{\mathrm{d}}^T\otimes\mathbf{R}_{\mathrm{d}})^{-\frac{1}{2}}\frac{\partial \mathbf{r}_{\mathrm{d}}}{\partial \boldsymbol{\theta}^T},\\ \mathbf{Q}_d &= (\mathbf{R}_{\mathrm{d}}^T\otimes\mathbf{R}_{\mathrm{d}})^{-\frac{1}{2}}\left[\frac{\partial \mathbf{r}_{\mathrm{d}}}{\partial \boldsymbol{\mu}^T}, \frac{\partial \mathbf{r}_{\mathrm{d}}}{\partial \sigma^2}\right].\end{aligned} \tag{24}$$

The dimensions of $\mathbf{G}_d$ and $\mathbf{Q}_d$ are $M^2 \times N$ and $M^2 \times (N+1)$, respectively. Then, the CRB for $\boldsymbol{\theta}$ can be expressed as

$$\mathrm{CRB}_{\mathrm{d}}(\boldsymbol{\theta}) = \frac{1}{K}(\mathbf{G}_{\mathrm{d}}^H \boldsymbol{\Pi}_{\mathbf{Q}_{\mathrm{d}}}^{\perp} \mathbf{G}_{\mathrm{d}})^{-1}, \tag{25}$$

with

$$\boldsymbol{\Pi}_{\mathbf{Q}_{\mathrm{d}}}^{\perp} = \mathbf{I}_{M^2} - \mathbf{Q}_{\mathrm{d}}(\mathbf{Q}_{\mathrm{d}}^H \mathbf{Q}_{\mathrm{d}})^{-1}\mathbf{Q}_{\mathrm{d}}^H. \tag{26}$$

Equation (25) coincides with those derived in [4], [5].

2) All the source signals are known to be noncircular (possibly strictly noncircular). In this case, $N_{\mathrm{c}} = 0$, and $N_{\mathrm{nc}} = N$. Therefore, $\boldsymbol{\psi}$ and $\boldsymbol{\rho}$ in (10) are augmented, so that the new $\mathbf{Q}_{e2}$ has a dimension of $4M^2 \times (3N+1)$. Substituting $\mathbf{Q}_{e2}$ into (22) instead of $\mathbf{Q}_e$ leads to a closed-form CRB expression for noncircular signals only.
3) The sources signals are known to be a mixture of circular and strictly noncircular ones. For strictly noncircular signals, $\rho_i = 1$, $i = 1, 2, \ldots, N_{\mathrm{nc}}$. Therefore, $\partial \mathbf{r}_{\mathrm{e}}/\partial \boldsymbol{\rho}$ can be removed from $\mathbf{Q}_{\mathrm{e}}$, and the newly constructed $\mathbf{Q}_{e3}$ is

$$\mathbf{Q}_{e3} = (\mathbf{R}_{\mathrm{e}}^T \otimes \mathbf{R}_{\mathrm{e}})^{-\frac{1}{2}} \left[\frac{\partial \mathbf{r}_{\mathrm{e}}}{\partial \boldsymbol{\mu}^T}, \frac{\partial \mathbf{r}_{\mathrm{e}}}{\partial \boldsymbol{\psi}^T}, \frac{\partial \mathbf{r}_{\mathrm{e}}}{\partial \sigma^2} \right]. \tag{27}$$

whose dimension is $\mathbf{Q}_{e3}$ is $4M^2 \times (N + N_{\mathrm{nc}} + 1)$. Substitute $\mathbf{Q}_{e3}$ into (22) instead of $\mathbf{Q}_{\mathrm{e}}$, and then the CRB for a mixture of circular and strictly noncircular signals can be obtained.
4) All the source signals are known to be strictly noncircular. In this case, $N_{\mathrm{c}} = 0$, $N_{\mathrm{nc}} = N$, and $\rho_i = 1$, $i = 1, 2, \ldots, N$. Hence, $\partial \mathbf{r}_{\mathrm{e}}/\partial \boldsymbol{\rho}$ can be removed from $\mathbf{Q}_{\mathrm{e}}$, and now the newly constructed $\mathbf{Q}_{e3}$ in (27) has a dimension of $4M^2 \times (2N+1)$. Note that another closed-form expression for the stochastic CRB in this case has been derived in [11, Theorem 2]. This CRB expression and its many related notations will not be shown here, but it is worth noting that this result is derived from a general expression [11, Eq. (10)], which is the same as in (22). Although the CRB expression in [11, Theorem 2] is more explicit than that in (22), it only applies to cases where $K<2M$, due to the usage of certain algebra results that only holds true in this region.

For some noncircular signals that do not follow the Gaussian distribution, the corresponding CRB should be derived based on the true p.d.f. rather than the Gaussian one, see, e.g., [10], [14], [15], [15], [15]. Fortunately, as proved in [10], the circular and noncircular Gaussian CRBs are tight upper bound on the CRBs for discrete QPSK and BPSK signals, respectively, at very low and very high signal-to-noise ratios (SNRs). Therefore, the above derived results can still provide a meaningful reference for nonGaussian signals.

IV. EXISTENCE OF THE DERIVED CRB BASED ON SPARSE ARRAYS

The existence of the derived CRB depends on the positive definiteness of $\mathbf{Q}_{\mathrm{e}}^H \mathbf{Q}_{\mathrm{e}}$ and $\mathbf{G}_{\mathrm{e}}^H \boldsymbol{\Pi}_{\mathbf{Q}_{\mathrm{e}}}^{\perp} \mathbf{G}_{\mathrm{e}}$, which further depends on the steering vector $\mathbf{a}(\theta_i)$. Since we aim to derive a bound for assessing the performance of some newly proposed algorithms based on sparse arrays, we shall focus on the application involving sparse arrays.

Consider a sparse array consisting of M sensors whose positions are represented by $\{p_1 d, p_2 d, \ldots, p_M d\}$, with p_m, $m = 1, 2, \ldots, M$ being an integer and d being the unit inter-element spacing. Typically, d is chosen to be half of the signal wavelength $\lambda/2$. Hereafter, we use the normalized DOA $\bar{\theta}_i = 2\pi d \sin\theta_i/\lambda$, $i = 1, 2, \ldots, N$ to replace the original DOA θ_i. Then, the steering vector corresponding to the ith source can be written as

$$\mathbf{a}(\bar{\theta}_i) = \left[\mathrm{e}^{\mathrm{j}p_1\bar{\theta}_i}, \mathrm{e}^{\mathrm{j}p_2\bar{\theta}_i} \ldots, \mathrm{e}^{\mathrm{j}p_M\bar{\theta}_i} \right]^T. \tag{28}$$

For a fixed $\bar{\theta}_i$, remove the repeated rows in $\mathbf{a}^*(\bar{\theta}_i) \otimes \mathbf{a}(\bar{\theta}_i)$ and $\mathbf{a}(\bar{\theta}_i) \otimes \mathbf{a}(\bar{\theta}_i)$ respectively, and then permute the unique rows according to an ascending order of the spatial lags. As a result, we can obtain two virtual steering vectors $\mathbf{v}_{\mathrm{d}}(\bar{\theta}_i)$ and $\mathbf{v}_{\mathrm{s}}(\bar{\theta}_i)$. Introduce the following matrices

$$\begin{aligned} \mathbf{V}_{\mathrm{d}}(\bar{\boldsymbol{\theta}}) &= [\mathbf{v}_{\mathrm{d}}(\bar{\theta}_1), \mathbf{v}_{\mathrm{d}}(\bar{\theta}_2), \ldots, \mathbf{v}_{\mathrm{d}}(\bar{\theta}_N)], \\ \mathbf{V}_{\mathrm{s}}(\bar{\boldsymbol{\theta}}_{\mathrm{nc}}) &= [\mathbf{v}_{\mathrm{s}}(\bar{\theta}_1), \mathbf{v}_{\mathrm{s}}(\bar{\theta}_2), \ldots, \mathbf{v}_{\mathrm{s}}(\bar{\theta}_{N_{\mathrm{nc}}})]. \end{aligned} \tag{29}$$

As such, $\mathbf{V}_{\mathrm{d}}(\bar{\boldsymbol{\theta}})$ and $\mathbf{V}_{\mathrm{s}}(\bar{\boldsymbol{\theta}}_{\mathrm{nc}})$ represent the steering matrices of the difference co-array and the sum co-array, respectively.

Denote the lengths of $\mathbf{v}_{\mathrm{d}}(\bar{\theta}_i)$ and $\mathbf{v}_{\mathrm{s}}(\bar{\theta}_i)$ as C_{d} and C_{s} respectively, which can be seen as the sensor numbers of the difference co-array and the sum co-array. Let $\mathbf{l}_{\mathrm{d}}$ and $\mathbf{l}_{\mathrm{s}}$ hold the spatial lags corresponding to $\mathbf{v}_{\mathrm{d}}(\bar{\theta}_i)$ and $\mathbf{v}_{\mathrm{s}}(\bar{\theta}_i)$, respectively. Then, we have

$$\begin{aligned} \mathbf{v}_{\mathrm{d}}(\bar{\theta}_i) &= \left[\mathrm{e}^{-\mathrm{j}\frac{C_{\mathrm{d}}-1}{2}\bar{\theta}_i}, \ldots, \mathrm{e}^{\mathrm{j}\frac{C_{\mathrm{d}}-1}{2}\bar{\theta}_i} \right]^T, \\ \mathbf{v}_{\mathrm{s}}(\bar{\theta}_i) &= \left[\mathrm{e}^{\mathrm{j}\Delta p\bar{\theta}_i}, \ldots, \mathrm{e}^{\mathrm{j}(\Delta p + C_{\mathrm{s}} - 1)\bar{\theta}_i} \right]^T, \\ \mathbf{l}_{\mathrm{d}} &= \left[-\frac{C_{\mathrm{d}}-1}{2}, \ldots, \frac{C_{\mathrm{d}}-1}{2} \right]^T, \\ \mathbf{l}_{\mathrm{s}} &= [\Delta p, \ldots, \Delta p + C_{\mathrm{s}} - 1]^T, \end{aligned} \tag{30}$$

where Δp is the smallest spatial lag in $\mathbf{v}_{\mathrm{s}}(\bar{\theta}_i)$. Note that the expressions of $\mathbf{l}_{\mathrm{d}}$ and $\mathbf{l}_{\mathrm{s}}$ in (30) are intended to show the first and last elements rather than implying that they contain consecutive integers.

The following relationships will be useful

$$\begin{aligned} \mathbf{a}^*(\bar{\theta}_i) \otimes \mathbf{a}(\bar{\theta}_i) &= \mathbf{J}_{\mathrm{d}}\mathbf{v}_{\mathrm{d}}(\bar{\theta}_i), \\ \mathbf{a}(\bar{\theta}_i) \otimes \mathbf{a}(\bar{\theta}_i) &= \mathbf{J}_{\mathrm{s}}\mathbf{v}_{\mathrm{s}}(\bar{\theta}_i), \end{aligned} \tag{31}$$

where $\mathbf{J}_{\mathrm{d}}$ and $\mathbf{J}_{\mathrm{s}}$ are $M^2 \times C_{\mathrm{d}}$ and $M^2 \times C_{\mathrm{s}}$ real-valued matrices of full column rank. The construction method of $\mathbf{J}_{\mathrm{d}}$ can be

found in [4, Appendix D], and $\mathbf{J}_{\mathrm{s}}$ can be constructed similarly. Therefore, we have

$$\begin{aligned}\mathbf{T}_{\mathrm{d}}(\bar{\boldsymbol{\theta}}) &= \mathbf{J}_{\mathrm{d}}\mathbf{V}_{\mathrm{d}}(\bar{\boldsymbol{\theta}}), \quad \mathbf{T}'_{\mathrm{d}}(\bar{\boldsymbol{\theta}}) = \mathrm{j}\mathbf{J}_{\mathrm{d}}\mathrm{diag}(\mathbf{l}_{\mathrm{d}})\mathbf{V}_{\mathrm{d}}(\bar{\boldsymbol{\theta}}),\\ \mathbf{T}_{\mathrm{s}}(\bar{\boldsymbol{\theta}}_{\mathrm{nc}}) &= \mathbf{J}_{\mathrm{s}}\mathbf{V}_{\mathrm{s}}(\bar{\boldsymbol{\theta}}_{\mathrm{nc}}), \ \mathbf{T}'_{\mathrm{s}}(\bar{\boldsymbol{\theta}}_{\mathrm{nc}}) = \mathrm{j}\mathbf{J}_{\mathrm{s}}\mathrm{diag}(\mathbf{l}_{\mathrm{s}})\mathbf{V}_{\mathrm{s}}(\bar{\boldsymbol{\theta}}_{\mathrm{nc}}).\end{aligned} \tag{32}$$

According to [4, Corollary 3],

$$\mathrm{vec}(\mathbf{I}_M) = \mathbf{J}_{\mathrm{d}}\mathbf{h}_{\mathrm{d}}, \tag{33}$$

where $\mathbf{h}_{\mathrm{d}}$ is a column vector whose pth element is given by $[\mathbf{h}_{\mathrm{d}}]_p = \delta_{[\mathbf{1}_{d}]p,0}, \forall p \in \mathbf{l}_{\mathrm{d}}$, with $\delta_{[\mathbf{1}_{d}]p,0}$ denoting the Kronecker function.

Using (19), (20), (32), and (33), we can rewrite $\mathbf{G}_{\mathrm{e}}$ and $\mathbf{Q}_{\mathrm{e}}$ as

$$\begin{aligned}\mathbf{G}_{\mathrm{e}} &= \mathrm{j}\mathbf{W}_{\mathrm{e}}\mathbf{P}\mathbf{J}\mathbf{L}\mathbf{U}_1,\\ \mathbf{Q}_{\mathrm{e}} &= \mathbf{W}_{\mathrm{e}}\mathbf{P}\mathbf{J}\mathbf{U}_2,\end{aligned} \tag{34}$$

where

$$\mathbf{J} = \begin{bmatrix} \mathbf{J}_{\mathrm{d}} & \mathbf{0}_{M^2\times C_{\mathrm{s}}} & \mathbf{0}_{M^2\times C_{\mathrm{s}}} & \mathbf{0}_{M^2\times C_{\mathrm{d}}} \\ \mathbf{0}_{M^2\times C_{\mathrm{d}}} & \mathbf{J}_{\mathrm{s}} & \mathbf{0}_{M^2\times C_{\mathrm{s}}} & \mathbf{0}_{M^2\times C_{\mathrm{d}}} \\ \mathbf{0}_{M^2\times C_{\mathrm{d}}} & \mathbf{0}_{M^2\times C_{\mathrm{s}}} & \mathbf{J}_{\mathrm{s}} & \mathbf{0}_{M^2\times C_{\mathrm{d}}} \\ \mathbf{0}_{M^2\times C_{\mathrm{d}}} & \mathbf{0}_{M^2\times C_{\mathrm{s}}} & \mathbf{0}_{M^2\times C_{\mathrm{s}}} & \mathbf{J}_{\mathrm{d}} \end{bmatrix},$$

$$\mathbf{L} = \begin{bmatrix} \mathrm{diag}(\mathbf{l}_{\mathrm{d}}) & \mathbf{0}_{C_{\mathrm{s}}\times C_{\mathrm{s}}} & \mathbf{0}_{C_{\mathrm{s}}\times C_{\mathrm{s}}} & \mathbf{0}_{C_{\mathrm{d}}\times C_{\mathrm{d}}} \\ \mathbf{0}_{C_{\mathrm{d}}\times C_{\mathrm{d}}} & \mathrm{diag}(\mathbf{l}_{\mathrm{s}}) & \mathbf{0}_{C_{\mathrm{s}}\times C_{\mathrm{s}}} & \mathbf{0}_{C_{\mathrm{d}}\times C_{\mathrm{d}}} \\ \mathbf{0}_{C_{\mathrm{d}}\times C_{\mathrm{d}}} & \mathbf{0}_{C_{\mathrm{s}}\times C_{\mathrm{s}}} & \mathrm{diag}(\mathbf{l}_{\mathrm{s}}) & \mathbf{0}_{C_{\mathrm{d}}\times C_{\mathrm{d}}} \\ \mathbf{0}_{C_{\mathrm{d}}\times C_{\mathrm{d}}} & \mathbf{0}_{C_{\mathrm{s}}\times C_{\mathrm{s}}} & \mathbf{0} & \mathrm{diag}(\mathbf{l}_{\mathrm{d}}) \end{bmatrix}, \tag{35}$$

while $\mathbf{U}_1$ and $\mathbf{U}_2$ are given by (36), as shown at the bottom of the page.

Notice that $\mathbf{G}_{\mathrm{e}}$ and $\mathbf{Q}_{\mathrm{e}}$ in (34) are similar to the matrices $\mathbf{G}$ and Δ in [4], and $\mathbf{W}_{\mathrm{e}}\mathbf{P}\mathbf{J}$ has full column rank. Following the proof of [4, Therorem 1], the existence condition of the CRB can be derived as

1) $\mathbf{Q}_{\mathrm{e}}^H\mathbf{Q}_{\mathrm{e}}$ is positive definite if and only if $\mathbf{U}_2$ has full column rank, i.e.,

$$\mathrm{rank}(\mathbf{U}_2) = 3N_{\mathrm{nc}} + N_{\mathrm{c}} + 1. \tag{37}$$

2) $\mathbf{G}_{\mathrm{e}}^H\boldsymbol{\Pi}_{\mathbf{Q}_{\mathrm{e}}}^{\perp}\mathbf{G}_{\mathrm{e}}$ is positive definite if and only if $[\mathrm{j}\mathbf{L}\mathbf{U}_1, \mathbf{U}_2]$ has full column rank, i.e,

$$\mathrm{rank}(\mathbf{G}_{\mathrm{e}}^H\boldsymbol{\Pi}_{\mathbf{Q}_{\mathrm{e}}}^{\perp}\mathbf{G}_{\mathrm{e}}) = 4N_{\mathrm{nc}} + 2N_{\mathrm{c}} + 1. \tag{38}$$

Since $\mathbf{U}_2$ and $[\mathrm{j}\mathbf{L}\mathbf{U}_1, \mathbf{U}_2]$ both have $2C_{\mathrm{d}}+2C_{\mathrm{s}}$ rows, the above rank conditions hold only if

$$4N_{\mathrm{nc}} + 2N_{\mathrm{c}} + 1 \le 2C_{\mathrm{d}} + 2C_{\mathrm{s}}. \tag{39}$$

which is

$$2N_{\mathrm{nc}} + N_{\mathrm{c}} \le C_{\mathrm{d}} + C_{\mathrm{s}} - \frac{1}{2}. \tag{40}$$

It is well-known that under the Gaussian distribution, the nonsingularity of the FIM, or the existence of the CRB, implies local identifiability of the unknown parameters [49]. Thus, (40) implies an upper bound (not guaranteed to be tight) on the number of (noncircular) signals that can be estimated by a specific sparse array. From the structure of $\mathbf{U}_1$ and $\mathbf{U}_2$, we can see that the DOFs offered by the difference co-array is shared by both the circular and noncircular signals, whereas the sum co-array only provides DOFs for the noncircular signals. Thus, the total number of sources that can be resolved, N, is related to the length of the difference co-array C_{d}. On the other hand, the number of noncircular sources that can be resolved, N_{nc}, is concerned with the length of the sum co-array C_{s}. Note that C_{d} and C_{s} are determined by the array structure itself, regardless of the signals. To illustrate more on this point, we recall the four cases discussed in Sec. III-B.

1) All the source signals are known to be circular. In this case, $N_{\mathrm{nc}} = 0$ and $\mathbf{R}_{\mathrm{s}} = \mathbf{0}$, so that the sum co-array is not utilized. Accordingly, the blocks in $\mathbf{U}_1$ and $\mathbf{U}_2$ that are associated with $\mathbf{V}_{\mathrm{s}}(\bar{\boldsymbol{\theta}}_{\mathrm{nc}})$ should be removed. Moreover, since the spatial lags in $\mathbf{V}_{\mathrm{d}}(\bar{\boldsymbol{\theta}}_{\mathrm{nc}})$ and $\mathbf{V}_{\mathrm{d}}(\bar{\boldsymbol{\theta}}_{\mathrm{d}})$ are symmetric with respect to zero, and thus the number of linearly independent rows in the newly constructed $\mathbf{U}_1$ and $\mathbf{U}_2$ reduces from $2C_{\mathrm{d}}$ to C_{d}. As a result, (40) degenerates to $N_{\mathrm{c}} \le (C_{\mathrm{d}} - 1)/2$, which is the well-known result in [3], [4].
2) All the source signals are known to be noncircular (possibly strictly noncircular). In this case, $N_{\mathrm{c}} = 0$, and (40) changes to $N \le (C_{\mathrm{d}} + C_{\mathrm{s}})/2 - 1/4$. Considering $(C_{\mathrm{d}} + C_{\mathrm{s}})/2 - 1/4$ should be an integer, we have $N \le (C_{\mathrm{d}} + C_{\mathrm{s}})/2 - 1$ with C_{s} set to be $(C_{\mathrm{s}} - 1)$ when it is even. This is the maximum number of noncircular source signals distinguishable by a sparse array, and it coincides with the conclusion in [31]. Thus, the existence of the sum co-array can significantly increase the number of resolvable sources. This also indicates that

$$\mathbf{U}_1 = \begin{bmatrix} \mathbf{V}_{\mathrm{d}}(\bar{\boldsymbol{\theta}}_{\mathrm{nc}})\mathrm{diag}(\boldsymbol{\mu}_{\mathrm{nc}}) & \mathbf{V}_{\mathrm{d}}(\bar{\boldsymbol{\theta}}_{\mathrm{c}})\mathrm{diag}(\boldsymbol{\mu}_{\mathrm{c}}) \\ -\mathbf{V}_{\mathrm{s}}^*(\bar{\boldsymbol{\theta}}_{\mathrm{nc}})\mathrm{diag}(\boldsymbol{\mu}_{\mathrm{nc}})\mathrm{diag}(\boldsymbol{\rho})\mathrm{diag}(\boldsymbol{\psi}_{\mathrm{e}}^*) & \mathbf{0}_{C_{\mathrm{s}}\times N_{\mathrm{c}}} \\ \mathbf{V}_{\mathrm{s}}(\bar{\boldsymbol{\theta}}_{\mathrm{nc}})\mathrm{diag}(\boldsymbol{\mu}_{\mathrm{nc}})\mathrm{diag}(\boldsymbol{\rho})\mathrm{diag}(\boldsymbol{\psi}_{\mathrm{e}}) & \mathbf{0}_{C_{\mathrm{s}}\times N_{\mathrm{c}}} \\ -\mathbf{V}_{\mathrm{d}}^*(\bar{\boldsymbol{\theta}}_{\mathrm{nc}})\mathrm{diag}(\boldsymbol{\mu}_{\mathrm{nc}}) & -\mathbf{V}_{\mathrm{d}}^*(\bar{\boldsymbol{\theta}}_{\mathrm{c}})\mathrm{diag}(\boldsymbol{\mu}_{\mathrm{c}}) \end{bmatrix},$$

$$\mathbf{U}_2 = \begin{bmatrix} \mathbf{V}_{\mathrm{d}}(\bar{\boldsymbol{\theta}}_{\mathrm{nc}}) & \mathbf{V}_{\mathrm{d}}(\bar{\boldsymbol{\theta}}_{\mathrm{c}}) & \mathbf{0}_{C_{\mathrm{d}}\times N_{\mathrm{nc}}} & \mathbf{0}_{C_{\mathrm{d}}\times N_{\mathrm{nc}}} & \mathbf{h}_{\mathrm{d}} \\ \mathbf{V}_{\mathrm{s}}^*(\bar{\boldsymbol{\theta}}_{\mathrm{nc}})\mathrm{diag}(\boldsymbol{\rho})\mathrm{diag}(\boldsymbol{\psi}_{\mathrm{e}}^*) & \mathbf{0}_{C_{\mathrm{d}}\times N_{\mathrm{c}}} & -\mathrm{j}\mathbf{V}_{\mathrm{s}}^*(\bar{\boldsymbol{\theta}}_{\mathrm{nc}})\mathrm{diag}(\boldsymbol{\mu}_{\mathrm{nc}})\mathrm{diag}(\boldsymbol{\rho})\mathrm{diag}(\boldsymbol{\psi}_{\mathrm{e}}^*) & \mathbf{V}_{\mathrm{s}}^*(\bar{\boldsymbol{\theta}}_{\mathrm{nc}})\mathrm{diag}(\boldsymbol{\mu}_{\mathrm{nc}})\mathrm{diag}(\boldsymbol{\psi}_{\mathrm{e}}^*) & \mathbf{0}_{C_{\mathrm{s}}\times 1} \\ \mathbf{V}_{\mathrm{s}}(\bar{\boldsymbol{\theta}}_{\mathrm{nc}})\mathrm{diag}(\boldsymbol{\rho})\mathrm{diag}(\boldsymbol{\psi}_{\mathrm{e}}), & \mathbf{0}_{C_{\mathrm{d}\times N_{\mathrm{c}}}} & \mathrm{j}\mathbf{V}_{\mathrm{s}}(\bar{\boldsymbol{\theta}}_{\mathrm{nc}})\mathrm{diag}(\boldsymbol{\mu}_{\mathrm{nc}})\mathrm{diag}(\boldsymbol{\rho})\mathrm{diag}(\boldsymbol{\psi}_{\mathrm{e}}) & \mathbf{V}_{\mathrm{s}}(\bar{\boldsymbol{\theta}}_{\mathrm{nc}})\mathrm{diag}(\boldsymbol{\mu}_{\mathrm{nc}})\mathrm{diag}(\boldsymbol{\psi}_{\mathrm{e}}) & \mathbf{0}_{C_{\mathrm{s}}\times 1} \\ \mathbf{V}_{\mathrm{d}}^*(\bar{\boldsymbol{\theta}}_{\mathrm{nc}}) & \mathbf{V}_{\mathrm{d}}^*(\bar{\boldsymbol{\theta}}_{\mathrm{c}}) & \mathbf{0}_{C_{\mathrm{d}}\times N_{\mathrm{nc}}} & \mathbf{0}_{C_{\mathrm{d}}\times N_{\mathrm{nc}}} & \mathbf{h}_{\mathrm{d}} \end{bmatrix}. \tag{36}$$

the CRB expression derived in this paper is applicable to cases where $M \leq N$, whereas the CRB expressions in [7], [8] are not.

3) The sources signals are known to be a mixture of circular and strictly noncircular ones. In this case, $\partial \mathbf{r}_e/\partial \boldsymbol{\rho}$ is removed from $\mathbf{Q}_e$, and the rank condition becomes $\text{rank}(\mathbf{U}_2) = 2N_{nc} + N_c + 1$ and $\text{rank}(\mathbf{G}_e^H \boldsymbol{\Pi}_{\mathbf{Q}_e}^{\perp} \mathbf{G}_e) = 3N_{nc} + 2N_c + 1$. Thus, these rank conditions hold only if $3N_{nc} + 2N_c + 1 \leq 2C_d + 2C_s$.
4) All the source signals are known to be strictly noncircular. In this case, $\partial \mathbf{r}_e/\partial \boldsymbol{\rho}$ is removed from $\mathbf{Q}_e$, with $N_c = 0$ and $N_{nc} = N$. Therefore, the rank conditions hold only if $N \leq (2C_d + 2C_s - 1)/3$, which means that more strictly noncircular sources can be resolved than the general all-noncircular case.

V. NUMERICAL RESULTS

In this section, results for the derived CRB_e in (23), the existing CRB for circular signals CRB_d in (26), and the CRB proposed by Delmas CRB_{Del} [10] are presented for comparison. All three types of signals are considered: circular signal ($\rho_i = 0$ and $\psi_i = 0$), strictly noncircular signal ($\rho_i = 1$ and $\psi_i = 0$), and nonstrictly noncircular signal ($\rho_i = 0.6$ and $\psi_i = 0$). The source powers of all the signals μ_i are equal. Symbols C, N_s and N_n are used in the rest of this section to represent circular signals, strictly noncircular signals, and nonstrictly noncircular signals, separately, and the number in front of the signal-type symbol represents the number of signals. For example, $1\text{N}_s2\text{C}$ means a mixture of one strictly noncircular and two circular signals. A six-sensor two-level nested array is employed, whose locations are $\{1, 2, 3, 4, 8, 12\}d$. The average CRB of all the impinging angles in degrees is recorded in every simulation.

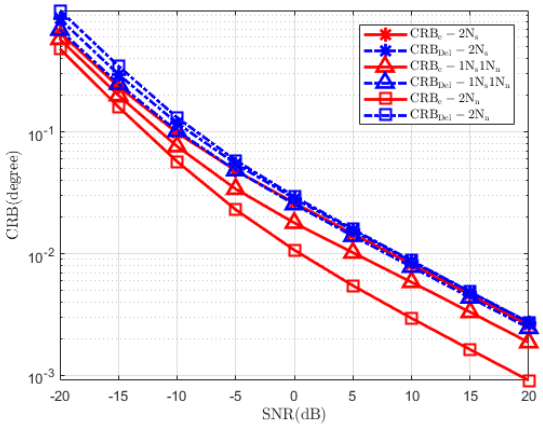

FIGURE 1. CRB results for different noncircular signal mixtures with a varying SNR at 5000 snapshots.

First, the CRBs of noncircular signals are studied using CRB_e and CRB_{Del}. There are two signals from $\theta_1 = -4°$ and $\theta_2 = 4°$, and they are divided into three scenarios: 2N_s, $1\text{N}_s1\text{N}_n$ and 2N_n. The number of snapshots is set to 5000, and SNR varies from -20dB to 20dB. The results for CRB_e and CRB_{Del} are shown in Fig. 1. Then, we fix SNR to 5dB and change the number of snapshots from 50 to 15000. The corresponding results are shown in Fig. 2.

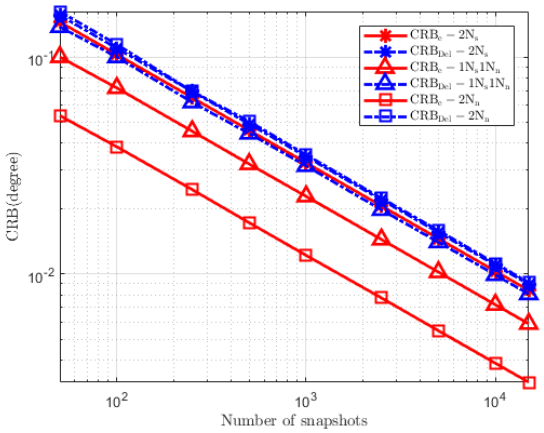

FIGURE 2. CRB results for different noncircular signal mixtures with a varying number of snapshots at 5dB SNR.

From the two figures, we can see that, for the three scenarios using CRB_{Del}, the CRB of $1\text{N}_s1\text{N}_n$ is the lowest while the CRB of 2N_n is the highest, but for CRB_e, the CRB of 2N_n is the lowest while the CRB of 2N_s is the highest. This is because CRB_{Del} and CRB_e are derived based on different parameterizations, as mentioned in *Remark 1*. In the same scenario, CRB_e is always lower than CRB_{Del}, and in particular, CRB_e and CRB_{Del} are almost the same in the 2N_s scenario. Compared with CRB_{Del}, CRB_e highlights the roles of the noncircularity phase and the noncircularity rate, and improves the potential estimation accuracy.

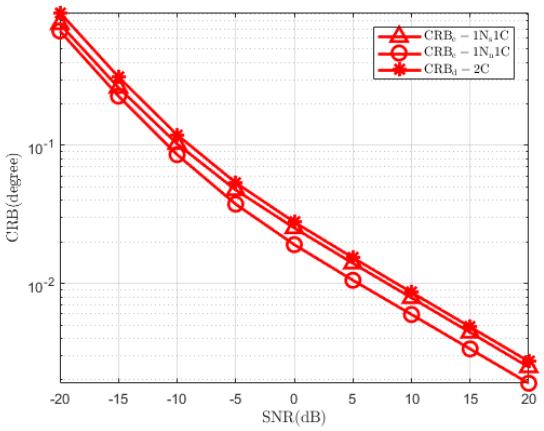

FIGURE 3. CRB results for different circular and noncircular signal mixtures with a varying SNR at 5000 snapshots.

In the second set of results, the CRBs for a mixture of circular and noncircular signals calculated from CRB_e and the CRB of circular signals calculated from CRB_d are studied. Still using the angles $\theta_1 = -4°$ and $\theta_2 = 4°$ as the mixture of circular and noncircular signals, and they are divided into two scenarios: $1\text{N}_s1\text{C}$ and $1\text{N}_n1\text{C}$. The number of snapshots is also set to 5000, and the CRB results with SNR varying from -20dB to 20dB are shown in Fig. 3. Then, SNR is fixed

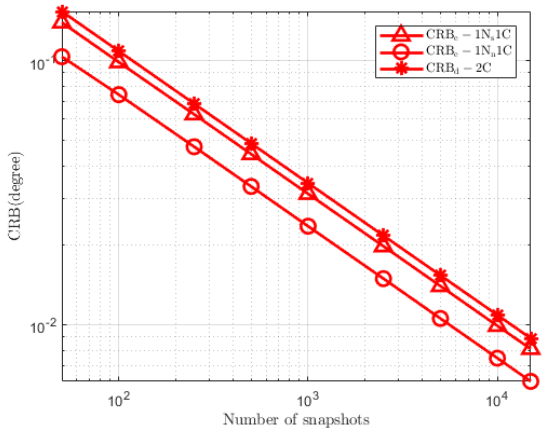

FIGURE 4. CRB results for different circular and noncircular signal mixtures with a varying number of snapshots at 5dB SNR.

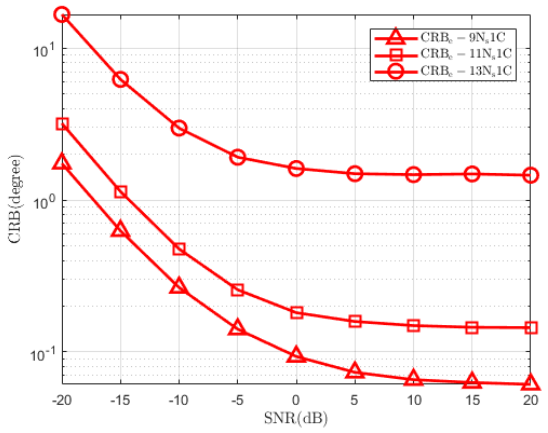

FIGURE 5. CRB results for different number of signals with a varying SNR at 5000 snapshots.

at 5dB, and the CRB results with the number of snapshots changing from 50 to 15000 are shown in Fig. 4.

From these two figures, we can see that the curve of $\mathrm{CRB_d}$ is always higher than the other curves, and the CRB of $1\mathrm{N_n}1\mathrm{C}$ is lower than the CRB of $1\mathrm{N_s}1\mathrm{C}$. Overall, the results confirm that the estimation accuracy of nonstrictly noncircular signals is better than that of strictly noncircular signals even in the case of a mixture of circular and noncircular signals situation.

In the third set of results, different numbers of mixture signals are considered, where one is circular and the rest are nonstrictly noncircular. The sparse array can estimate at most a mixture of 14 circular and noncircular signals using the estimation algorithms proposed in [31], while the maximum number of circular signals can be estimated is 11 [24]. Then, three scenarios are examined: $9\mathrm{N_s}1\mathrm{C}$, $11\mathrm{N_s}1\mathrm{C}$ and $13\mathrm{N_s}1\mathrm{C}$. The DOAs are chosen as $\{\ldots, -12°, -4°, 4°, 12°, \ldots\}$ with 8° interval. For example, the set of DOAs is $\{-20°, -12°, -4°, 4°, 12°, 20°\}$ for 6 signals. The circular signal is always located at the largest DOA. The number of snapshots is also set to 5000 when SNR varies from −20dB to 20dB, and the results is shown in Fig. 5. Then, the SNR is also fixed at 5dB, and the number of snapshots varies from 50 to 15000, and the results is shown in Fig. 6.

From these two figures, we can see that $\mathrm{CRB_e}$ increases when the number of signals increases. Note that the numbers of sources are all set to be larger than that of physical sensors, which is referred to as the underdetermined case. In this situation, $\mathrm{CRB_e}$ will finally become almost a constant as SNR increases. The proposed $\mathrm{CRB_e}$ can handle the underdetermined situation, whereas $\mathrm{CRB_{Del}}$ cannot. Moreover, $\mathrm{CRB_e}$ exists even when the number of signals is greater than 11, which falls into the invalid range of $\mathrm{CRB_d}$. That means more noncircular signals can be resolved based on a given array, compared with the all-circular case [6].

In the fourth set of results, the total number of signals is fixed and underdetermined, while the number of circular signals varies. Three scenarios are examined: $8\mathrm{N_s}2\mathrm{C}$, $7\mathrm{N_s}3\mathrm{C}$ and $6\mathrm{N_s}4\mathrm{C}$. The DOAs are chosen as $\{-36°, -28°, -20°, -12°, -4°, 4°, 12°, 20°, 28°, 36°\}$. The settings of SNR and the number of snapshots are the same as before, and the results are shown in Figs. 7 and 8.

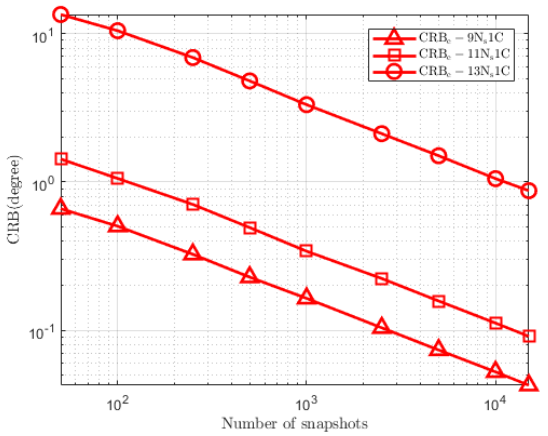

FIGURE 6. CRB results for different number of signals with a varying number of snapshots at 5dB SNR.

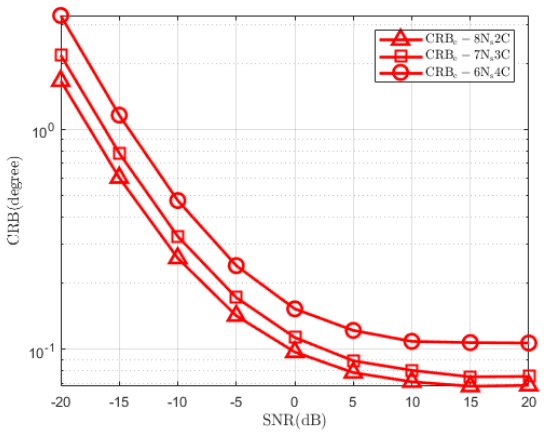

FIGURE 7. CRB results for different number of circular signals in the mixture with a varying SNR at 5000 snapshots.

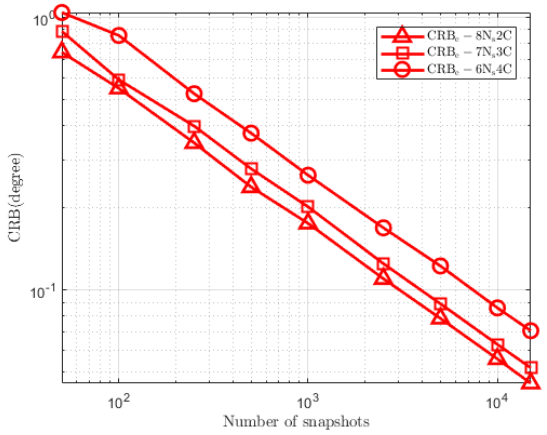

FIGURE 8. CRB results for different number of circular signals in the mixture with a varying number of snapshots at 5dB SNR.

From these two figures, we can see that CRB_e increases when the number of circular signals in the mixture increase, which confirms that the estimation accuracy of noncircular signals is better than that of circular ones even in the underdetermined situation. Moreover, as before, CRB_e decreases as the number of snapshots and SNR increase, and it reaches a constant state after SNR becomes higher than some value.

VI. CONCLUSION

In this paper, the stochastic CRB for a mixture of circular and noncircular uncorrelated Gaussian signals has been derived for the first time. Taking into account different *a priori* knowledge about noncircularity, the derived CRB can be transformed to cover several special cases, including the CRB for ULAs, CRB for noncircular signals only, CRB for a mixture of circular and strictly noncircular signals, and CRB for circular signals only. The existence condition of the CRB was examined in detail based on sparse arrays, with the number of resolvable sources discussed. Simulations were conducted in different scenarios, and the proposed CRB which considers the noncircularity property would lead to a lower value than those without. Furthermore, the proposed CRB was shown to be applicable to cases with more sources than the number of physical sensors.

REFERENCES

[1] P. Stoica and A. Nehorai, "MUSIC, maximum likelihood and Cramer-Rao bound," *IEEE Trans. Acoust., Speech, Signal Process.*, vol. 37, no. 5, pp. 720–741, May 1989.
[2] P. Stoica and A. Nehorai, "Performance study of conditional and unconditional direction-of-arrival estimation," *IEEE Trans. Acoust., Speech, Signal Process.*, vol. 38, no. 10, pp. 1783–1795, Jun. 1990.
[3] A. Koochakzadeh and P. Pal, "Cramér–Rao bounds for underdetermined source localization," *IEEE Signal Process. Lett.*, vol. 23, no. 7, pp. 919–923, Jul. 2016.
[4] C.-L. Liu and P. P. Vaidyanathan, "Cramér–Rao bounds for coprime and other sparse arrays, which find more sources than sensors," *Digit. Signal Process.*, vol. 61, pp. 43–61, Feb. 2017.
[5] M. Wang and A. Nehorai, "Coarrays, MUSIC, and the Cramér–Rao bound," *IEEE Trans. Signal Process.*, vol. 65, no. 4, pp. 933–946, Feb. 2017.
[6] Y. Liang, Q. Shen, W. Cui, and W. Liu, "Cramér-Rao bound for wideband DOA estimation with uncorrelated sources," in *Proc. IEEE Global Conf. Signal Inf. Process. (GlobalSIP)*, Ottawa, ON, Canada, Nov. 2019, pp. 1–5.
[7] H. Abeida and J. Delmas, "Gaussian Cramer-Rao bound for direction estimation of noncircular signals in unknown noise fields," *IEEE Trans. Signal Process.*, vol. 53, no. 12, pp. 2678–2690, Dec. 2005.
[8] J.-P. Delmas and H. Abeida, "Stochastic Cramér–Rao bound for noncircular signals with application to DOA estimation," *IEEE Trans. Signal Process.*, vol. 52, no. 11, pp. 3192–3199, Nov. 2004.
[9] Y. Liang, W. Liu, Q. Shen, W. Cui, and S. Wu, "A review of closed-form Cramér-Rao bounds for DOA estimation in the presence of Gaussian noise under a unified framework," *IEEE Access*, vol. 8, pp. 175101–175124, Sep. 2020.
[10] J.-P. Delmas and H. Abeida, "Cramer-Rao bounds of DOA estimates for BPSK and QPSK modulated signals," *IEEE Trans. Signal Process.*, vol. 54, no. 1, pp. 117–126, Jan. 2006.
[11] H. Abeida and J. P. Delmas, "Direct derivation of the stochastic CRB of DOA estimation for rectilinear sources," *IEEE Signal Process. Lett.*, vol. 24, no. 10, pp. 1522–1526, Oct. 2017.
[12] J. Steinwandt, F. Roemer, and M. Haardt, "Deterministic Cramér-Rao bound for a mixture of circular and strictly non-circular signals," in *Proc. Int. Symp. Wireless Commun. Syst. (ISWCS)*, Brussels, Belgium, Aug. 2015, pp. 661–665.
[13] Y.-H. Choi, "Cramér-Rao bounds for direction estimation in the presence of circular and noncirular signals," *IEEE Access*, vol. 8, pp. 177395–177404, Sep. 2020.
[14] H. Abeida and J.-P. Delmas, "Slepian–Bangs formula and Cramér–Rao bound for circular and non-circular complex elliptical symmetric distributions," *IEEE Signal Process. Lett.*, vol. 26, no. 10, pp. 1561–1565, Oct. 2019.
[15] H. Steendam and M. Moeneclaey, "Low-SNR limit of the Cramer-Rao bound for estimating the carrier phase and frequency of a PAM, PSK, or QAM waveform," *IEEE Commun. Lett.*, vol. 5, no. 5, pp. 218–220, May 2001.
[16] F. Wen, J. Shi, and Z. Zhang, "Joint 2D-DOD, 2D-DOA, and polarization angles estimation for bistatic EMVS-MIMO radar via PARAFAC analysis," *IEEE Trans. Veh. Technol.*, vol. 69, no. 2, pp. 1626–1638, Feb. 2020.
[17] F. Wen, X. Zhang, and Z. Zhang, "CRBs for direction-of-departure and direction-of-arrival estimation in collocated MIMO radar in the presence of unknown spatially coloured noise," *IET Radar, Sonar Navigat.*, vol. 13, no. 4, pp. 530–537, Apr. 2019.
[18] L. Wan, G. Han, L. Shu, and N. Feng, "The critical patients localization algorithm using sparse representation for mixed signals in emergency healthcare system," *IEEE Syst. J.*, vol. 12, no. 1, pp. 52–63, Mar. 2018.
[19] L. Wan, G. Han, J. Jiang, J. J. P. C. Rodrigues, N. Feng, and T. Zhu, "DOA estimation for coherently distributed sources considering circular and noncircular signals in massive MIMO systems," *IEEE Syst. J.*, vol. 11, no. 1, pp. 41–49, Mar. 2017.
[20] M. La Manna and D. R. Fuhrmann, "Cramér–Rao lower bounds comparison for 2D hybrid–MIMO and MIMO radar," *IEEE J. Sel. Topics Signal Process.*, vol. 11, no. 2, pp. 404–413, Mar. 2017.
[21] P. P. Vaidyanathan and P. Pal, "Sparse sensing with co-prime samplers and arrays," *IEEE Trans. Signal Process.*, vol. 59, no. 2, pp. 573–586, Feb. 2011.
[22] S. Qin, Y. D. Zhang, and M. G. Amin, "Generalized coprime array configurations for direction-of-arrival estimation," *IEEE Trans. Signal Process.*, vol. 63, no. 6, pp. 1377–1390, Mar. 2015.
[23] A. Raza, W. Liu, and Q. Shen, "Thinned coprime array for second-order difference co-array generation with reduced mutual coupling," *IEEE Trans. Signal Process.*, vol. 67, no. 8, pp. 2052–2065, Apr. 2019.
[24] P. Pal and P. P. Vaidyanathan, "Nested arrays: A novel approach to array processing with enhanced degrees of freedom," *IEEE Trans. Signal Process.*, vol. 58, no. 8, pp. 4167–4181, Aug. 2010.
[25] C.-L. Liu and P. P. Vaidyanathan, "Super nested arrays: Linear sparse arrays with reduced mutual coupling—Part I: Fundamentals," *IEEE Trans. Signal Process.*, vol. 64, no. 15, pp. 3997–4012, Aug. 2016.
[26] C.-L. Liu and P. P. Vaidyanathan, "Remarks on the spatial smoothing step in coarray MUSIC," *IEEE Signal Process. Lett.*, vol. 22, no. 9, pp. 1438–1442, Sep. 2015.

[27] Q. Shen, W. Liu, W. Cui, S. Wu, Y. D. Zhang, and M. G. Amin, "Low-complexity direction-of-arrival estimation based on wideband co-prime arrays," *IEEE/ACM Trans. Audio, Speech, Lang. Process.*, vol. 23, no. 9, pp. 1445–1456, Sep. 2015.

[28] J. Cai, D. Bao, P. Li, J. Cai, D. Bao, and P. Li, "DOA estimation via sparse recovering from the smoothed covariance vector," *J. Syst. Eng. Electron.*, vol. 27, no. 3, pp. 555–561, Jun. 2016.

[29] Z. Shi, C. Zhou, Y. Gu, N. A. Goodman, and F. Qu, "Source estimation using coprime array: A sparse reconstruction perspective," *IEEE Sensors J.*, vol. 17, no. 3, pp. 755–765, Feb. 2017.

[30] J. Cai, W. Liu, R. Zong, and Q. Shen, "An expanding and shift scheme for constructing fourth-order difference coarrays," *IEEE Signal Process. Lett.*, vol. 24, no. 4, pp. 480–484, Apr. 2017.

[31] J. Cai, W. Liu, R. Zong, and B. Wu, "Sparse array extension for non-circular signals with subspace and compressive sensing based DOA estimation methods," *Signal Process.*, vol. 145, pp. 59–67, Apr. 2018.

[32] J. Cai, W. Liu, R. Zong, and B. Wu, "An improved expanding and shift scheme for the construction of fourth-order difference co-arrays," *Signal Process.*, vol. 153, pp. 95–100, Dec. 2018.

[33] P. Chargé, Y. Wang, and J. Saillard, "A non-circular sources direction finding method using polynomial rooting," *Signal Process.*, vol. 81, no. 8, pp. 1765–1770, Aug. 2001.

[34] J. Liu, Z. Huang, and Y. Zhou, "Extended 2q-MUSIC algorithm for noncircular signals," *Signal Process.*, vol. 88, no. 6, pp. 1327–1339, Jun. 2008.

[35] H. Abeida and J.-P. Delmas, "Statistical performance of MUSIC-like algorithms in resolving noncircular sources," *IEEE Trans. Signal Process.*, vol. 56, no. 9, pp. 4317–4329, Sep. 2008.

[36] Z. T. Huang, Z. M. Liu, J. Liu, and Y. Y. Zhou, "Performance analysis of MUSIC for non-circular signals in the presence of mutual coupling," *IET Radar, Sonar Navigat.*, vol. 4, no. 5, pp. 703–711, 2010.

[37] J. Steinwandt, F. Roemer, M. Haardt, and G. D. Galdo, "R-dimensional ESPRIT-type algorithms for strictly second-order non-circular sources and their performance analysis," *IEEE Trans. Signal Process.*, vol. 62, no. 18, pp. 4824–4838, Sep. 2014.

[38] H. Chen, C. Hou, W. Liu, W. Zhu, and M. Swamy, "Efficient two-dimensional direction of arrival estimation for a mixture of circular and noncircular sources," *IEEE Sensors J.*, vol. 16, no. 8, pp. 2527–2536, Apr. 2016.

[39] F. Gao, A. Nallanathan, and Y. Wang, "Improved MUSIC under the coexistence of both circular and noncircular sources," *IEEE Trans. Signal Process.*, vol. 56, no. 7, pp. 3033–3038, Jul. 2008.

[40] J. Steinwandt, F. Roemer, M. Haardt, and G. D. Galdo, "Deterministic Cramér-Rao bound for strictly non-circular sources and analytical analysis of the achievable gains," *IEEE Trans. Signal Process.*, vol. 64, no. 17, pp. 4417–4431, Sep. 2016.

[41] Z.-M. Liu, Z.-T. Huang, Y.-Y. Zhou, and J. Liu, "Direction-of-arrival estimation of noncircular signals via sparse representation," *IEEE Trans. Aerosp. Electron. Syst.*, vol. 48, no. 3, pp. 2690–2698, Jul. 2012.

[42] X. Yang, G. Li, and Z. Zheng, "DOA estimation of noncircular signal based on sparse representation," *Wireless Pers. Commun.*, vol. 82, no. 4, pp. 2363–2375, Feb. 2015.

[43] J. Steinwandt, F. Roemer, and M. Haardt, "Sparsity-based direction-of-arrival estimation for strictly non-circular sources," in *Proc. IEEE Int. Conf. Acoust., Speech Signal Process. (ICASSP)*, Shanghai, China, Mar. 2016, pp. 3246–3250.

[44] P. Gupta and M. Agrawal, "Design and analysis of the sparse array for DoA estimation of noncircular signals," *IEEE Trans. Signal Process.*, vol. 67, no. 2, pp. 460–473, Jan. 2019.

[45] J. Steinwandt, F. Roemer, and M. Haardt, "ESPRIT-type algorithms for a received mixture of circular and strictly non-circular signals," in *Proc. IEEE Int. Conf. Acoust., Speech Signal Process. (ICASSP)*, Brisbane, QLD, Australia, Apr. 2015, pp. 2809–2813.

[46] Y. Tian, H. Yue, and X. Rong, "Multi-parameters estimation of coherently distributed sources under coexistence of circular and noncircular signals," *IEEE Commun. Lett.*, vol. 24, no. 6, pp. 1254–1257, Jun. 2020.

[47] D. Slepian, "Estimation of signal parameters in the presence of noise," *Trans. IRE Prof. Group Inf. Theory*, vol. 3, no. 3, pp. 68–89, Mar. 1954.

[48] W. J. Bangs, "Array processing with generalized beam-formers," Ph.D. dissertation, Yale Univ., New Haven, CT, USA, 1971.

[49] B. Hochwald and A. Nehorai, "On identifiability and information-regularity in parametrized normal distributions," *Circuits Syst. Signal Process.*, vol. 16, no. 1, pp. 83–89, Jan. 1997.

JINGJING CAI received the B.S. degree from the Beijing University of Posts and Telecommunications, Beijing, China, in 2006, and the Ph.D. degree from Xidian University, Xi'an, China, in 2014. From 2016 to 2017, she was an Academic Visitor with the Department of Electronic Electrical Engineering, The University of Sheffield, Sheffield, U.K. She is currently working as an Associate Professor with the School of Electronic and Engineering. Her research interest includes sensor array signal processing and its various applications, such as radar, sonar, and wireless communications.

YIBAO LIANG was born in Shandong, China, in 1994. He received the B.Eng. and B.B.A. degrees from the Beijing Institute of Technology, Beijing, China, in 2016, where he is currently pursuing the Ph.D. degree with the School of Information and Electronics. From October 2019 to March 2020, he was a Visiting Researcher with the Department of Electronic and Electrical Engineering, The University of Sheffield, Sheffield, U.K. His research interests include radar and array signal processing.

WEI LIU (Senior Member, IEEE) received the B.Sc. and LLB degrees from Peking University, China, in 1996 and 1997, respectively, the M.Phil. degree from The University of Hong Kong, in 2001, and the Ph.D. degree from the School of Electronics and Computer Science, University of Southampton, U.K., in 2003. He then held a postdoctoral position first with University of Southampton, and later with the Department of Electrical and Electronic Engineering, Imperial College London. Since September 2005, he has been with the Department of Electronic and Electrical Engineering, The University of Sheffield, U.K., first as a Lecturer and then a Senior Lecturer. He has published more than 300 journal and conference papers, five book chapters, and two research monographs titled *Wideband Beamforming: Concepts and Techniques* (John Wiley, March 2010) and *Low-Cost Smart Antennas* (Wiley-IEEE, March 2019). His research interest includes signal processing, with a focus on sensor array signal processing and its various applications, such as robotics and autonomous systems, human computer interface, radar, sonar, satellite navigation, and wireless communications.

He is a member of the Digital Signal Processing Technical Committee of the IEEE Circuits and Systems Society, and a Secretary, from May 2020. He has been a Vice Chair of the Sensor Array and Multichannel Signal Processing Technical Committee of the IEEE Signal Processing Society, since January 2019. He was an Associate Editor for IEEE TRANSACTIONS ON SIGNAL PROCESSING, from March 2015 to March 2019. He is currently an Associate Editor for IEEE ACCESS, and an Editorial Board Member of the journal *Frontiers of Information Technology and Electronics Engineering*.

YANG-YANG DONG (Member, IEEE) received the B.Eng. and Ph.D. degrees in electronic science and technology from Xidian University, Xi'an, China, in 2012 and 2017, respectively. Since 2017, he has been a Lecturer with the School of Electronic Engineering, Xidian University, where he also held a postdoctoral position. His current research interests include array signal processing, multilinear algebra, and information geometry.